NUKLEONIKA 2009;54(1):33–38

ORIGINAL PAPER

Preliminary design and simulation of a spherical brain PET system (SBPET) with liquid xenon as scintillator

Nayerehalsadat Mortazavi Moghaddam, Alireza Karimian, Seyed M. Mostajaboddavati, Eric Vondervoort, Vesna Sossi

Abstract. Preliminary design of a spherical brain PET (SBPET) using liquid xenon (LXe) as detector is considered in this research work. The major advantage of a spherical design is the large solid angle of acceptance which improves the sensitivity and increases signal-to-noise ratio (SNR) of the image. The use of a liquid active medium enabled us to design a spherical detector. LXe, due to the intrinsic physical properties, is an excellent liquid medium for accurate tracking of gamma rays in the relevant energy range. The performance of SBPET was evaluated by Monte Carlo simulation tools (GATE) and compared to ECAT HRRT. The numerical results showed the SBPET has a sensitivity of 1.14% and spatial resolution of ~2.7 mm FWHM which is superior to ECAT HRRT especially at high-count rates.

Key words: positron emission tomography (PET) • Monte Carlo simulation • GATE • liquid xenon • brain imaging

N. Mortazavi Moghaddam✉, S. M. Mostajaboddavati
Physics Department,
University of Isfahan,
Hezar jerib Ave., P. O. Box 81745-319,
Isfahan, Iran,
Tel.: +98 21 2212 7215, Fax: +98 21 8861 3937,
E-mail: mortazavi@alzahra.ac.ir

A. R. Karimian
Department of Biomedical Engineering,
Faculty of Engineering,
University of Isfahan,
Postal code: 81744,
Isfahan, Iran

E. Vondervoort, V. Sossi
Brain Research Centre,
UBC Hospital,
University of British Columbia,
2211 Wesbrook Mall,
Vancouver, Canada

Received: 10 March 2008
Accepted: 6 November 2008

Introduction

Due to the growing interest in brain investigations, a vast amount of research has been conducted including the study and development of accurate brain imaging techniques [15, 28, 32, 37]. While CT-scan and MRI systems are suitable for anatomical study of the brain, nuclear imaging systems such as gamma camera, single photon emission computed tomography (SPECT), and positron emission tomography (PET) are applied in physiological studies [17, 33]. PET with its high sensitivity and spatial resolution appears uniquely suited for quantification of brain functions such as blood flow, metabolism and receptor characteristics. This quantified information provides medical scientists and practitioners a much deeper understanding about many neurological and mental disorders.

In PET diagnosis technique, the patient under examination is injected a radiopharmaceutical compound (FDG) labeled with a β^+ emitting radionuclide. The annihilation of positron and electron creates two 511 KeV photons flying in opposite directions. The emitted photons interact with the scintillation material within the scanner detectors and the data obtained from the detectors for a large number of such events is used for reconstruction of positron emitter distribution [17, 36].

The grand challenge for advanced PET instrumentation is optimizing the performance in terms of sensitivity, spatial resolution and contrast as well as minimizing operation and fabrication costs. To achieve these objectives, a significant progress has been made in the design

Table 1. Properties of scintillation crystals used in PET [1, 10, 27, 38]

Scintillator	BGO	LSO	GSO	LYSO	LXe
Effective Z	75	66	60	64	54
Light yield (photon/MeV)	9000	25 000	8000	32 000	78 000
Decay time (ns)	300	42	60	48	2.2, 22
Peak wavelength (nm)	480	420	440	420	178
Index of refraction	2.15	1.82	1.95	1.8	1.6–1.72
Energy resolution (%)	12	9.1	7.9	7.1	22

of dedicated brain PET [6, 25, 28, 39] by either using different scintillation materials for detectors [10, 20, 21, 35] or by changing the geometry of the system [14, 23, 24]. In this work the idea of utilizing liquid xenon (LXe) as the detector material in a dedicated brain PET with spherical geometry is explored by means of Monte Carlo simulation tools. We use SBPET as an acronym for the proposed design in the course of this paper. SBPET stands for spherical brain PET.

Liquid xenon with its high scintillation yield and short decay time is a promising scintillator for a PET system [4, 5, 10, 12, 13, 18, 35]. A detailed comparison of the properties of LXe to the most commonly used scintillation crystals will be made in the first section of the paper.

Two gamma non-colinearity is one of the fundamental physical resolution limits in the PET system. Non-colinearity arises from the fact that two annihilated photons deviate from the exact 180 degree position, thus the observed line of response (LOR) between two detectors does not intersect the point of annihilation. Decrease in the distance between the two detectors decreases the non-colinearity effect [29].

In the clinical PET scanner (WB-PET) that is commonly used for brain imaging, the detectors are typically 20–30 cm away from the brain, which results in sensitivity reduction. In this work, by designing a spherical scanner in a dedicated brain PET we were able to reduce the scanner's ring diameter which increases the solid converge angle leading to a higher sensitivity per unit detector volume [24]. A small ring design has the advantage of decreasing non-colinearity effect of annihilation photons and reducing the overall cost. In addition, spherical scanner geometry has the benefit of large solid angle of acceptance, which leads to improved system sensitivity.

In PET system, the ultimate performance can be achieved through careful selection of the geometry, detector assembly and readout electronics and whose Monte Carlo simulations play an important role to assist these developments [3]. In this research work GEANT4, a Monte Carlo software toolkit, in conjunction with GATE [19, 30, 31], a simulation platform for tomographic emission application, is employed to assess the performance of the SBPET. At the end, the performance of the SBPET using LXe computed using the Monte Carlo method is compared to the performance of ECAT HRRT scanner reported in the literature.

Properties of liquid xenon

Scintillation detector is one of the most critical components of PET system. Most of the early dedicated brain PETs which were developed in the 1970's, employed NaI(TI) and CsF crystals as the detector material [9]. Positome II, which was designed and prototyped by Thompson [35] is an example of such systems. In the 1980's and 1990's many other PET systems were designed such as Hamamatsu SHR 1200/2400 and ECAT 953B. BGO and GSO crystals were used in these prototypes, respectively. Recently, LSO and LYSO crystals were used in high resolution research tomograph (HRRT). The characteristics of most commonly used scintillation crystals for the current generation PETs are listed and compared to LXe in Table 1 [26, 37].

The photons produced in the positron annihilation process interact with the detector through the Rayleigh, Compton scattering and photoelectric effects. Photoelectric and Compton cross-sections are directly proportional to the density ρ and effective atomic number Z_{eff} of the scintillation material. As a result, a high effective atomic number is desirable in for a scintillator. The decay time and light yield are other important factors for selecting the scintillator. Decay time is the most important factor to select the temporal coincidence window, which results in higher yield of random coincidence per unit activity especially at high-count rates. Light yield is directly connected to the spatial resolution of the detector, as higher light yield would improve the energy resolution.

LXe is a known gamma detection medium which features gamma interaction properties comparable to NaI(Tl). The physical properties of LXe are listed in Table 2. Based on the information presented in Tables 1 and 2, one can observe that LXe has many advantages over other scintillation materials. The scintillation efficiency of LXe is twice as high as that of NaI(Tl) and the light decay time is more than ten times faster than the best value of all crystals considered in PET (40 ns for LSO). Such fast decay times are important to achieve better time resolution at high counting rates. In addition, LXe has a high scintillation yield, low ionization potential and large light yields (9 times more than BGO and 3.5 times more than LSO). The density of LXe (3 g/cm^3) is lower than LSO, however it can be expanded easily in the depth direction (parallax free).

Materials and methods

In Fig. 1, a scheme of SBPET system is shown. The scanner consists of 36 × 5 blocks of liquid xenon module where the dimension of each block is 32 × 50 × 100 mm. Each module is optically divided into10 by using Mg-F2-coated aluminum UV light guides [16], each of them having a thickness of 3.2 mm as shown in Fig. 1. The axial field of view of the scanner is 25.0 cm with external and inter-

Table 2. Properties of liquid xenon [34]

Material properties	Value & unit	Conditions
Atomic number Z	54	
Atomic weight A	131.29 g/mole	
Boiling point *Tb*	165.1 K	1 atm
Melting point *Tm*	161.4	1 atm
Density ρ	2.98 g/cm^3	161.35 K
Critical point *Tc*, *Pc*	289.7 K, 58.4 bar	
Triple point *T3*, *P3*	161.3 K, 0.816 bar	
Refractive index	1.6–1.72	in liquid
Lifetime singlet	22 ns	
Lifetime triplet	4.2 ns	
Recombination time	45 ns	
Energy/scint. photon W ph	(23.7 ± 2.4) eV (19.6 ± .0) eV	electrons α-particles
Peak emission wavelength, λscint	178 nm	
Scient absorption length, λabs	> 100 cm	
Rayleigh scattering length, λR	(29 ± 2) cm	

nal port diameters of 58.0 cm and 38.0 cm, respectively. The size of scanner's port is suitable for an adult size human brain and the diameter of port is comparable with a 46.9 cm diameter of ECAT HRRT system [2]. For simulation purposes, a standard NEMA phantom is placed at the center of the scanner. The phantom is assumed to be a 20 cm long cylinder of water with a diameter of 20 cm. A 19 cm long line source with diameter of 1 mm is inserted inside and parallel to the axis of the water cylinder. The source is filled with F-18.

In the simulation, Rayleigh, Compton and photoelectric photon interactions are represented using GEANT4 low-energy photon models. These interactions are converted into counts by GATE signal processing tool known as "digitizer" [19]. A "dead time" module is inserted to create dead time at the block level which is triggered by the pulses within the block. Energy-window discriminator is applied via the thresholder and upholder modules. Finally, the coincidence module sorts the remaining pulses.

The tests described in these protocols measure a scanner scatter fraction, true, scattered and random coincidence count rates, sensitivity, spatial resolutions and image quality, from which, only the spatial resolutions test requires image reconstructions.

In the next section, the performance of the proposed PET design is assessed through a set of simulations.

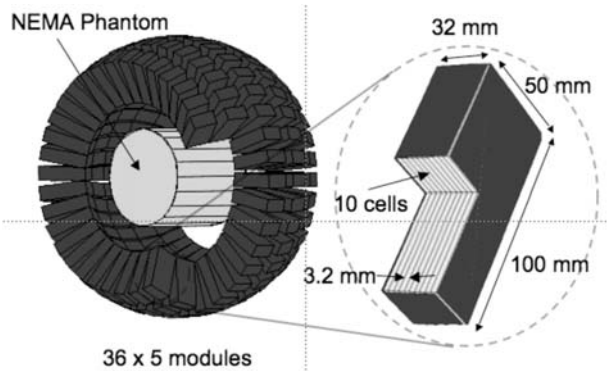

Fig. 1. Scheme of the SBPET (left). A blown up of a detector module (right).

Results

The objective of the first set of simulations is to find an optimal detector thickness. The thickness is varied from 20 to 140 mm and the sensitivity of the detector is measured. Sensitivity is defined as the number of counts per unit time detected by the device for each unit of activity present in the source. For each ring of the scanner, sensitivity S can be expressed as [29]:

$$S = A \cdot \varepsilon^2 \cdot \exp \cdot (-\mu t) \cdot 3.7 \times 10^4 / 4\varpi r^2, \quad (1)$$

In the above equation A is the projected area of the detector seen by a point source, ε is the efficiency of the detector, μ is the linear attenuation coefficient of photons in the detector material, t is the thickness of the detector and r is the radius of the detector ring.

The sensitivity as a function of thickness is shown in Fig. 2. As it can be observed, for the thicknesses greater than 100 mm the sensitivity grows very slowly. Based on this result and considering geometrical constraints, the thickness of 100 mm is selected for the detector; at this thickness the sensitivity is 1.14%. For this simulation, the energy resolution of LXe is set to 22% [5].

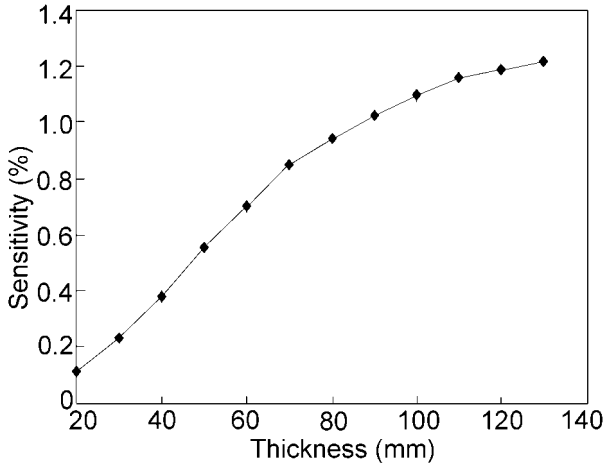

Fig. 2. Sensitivity of SBPET vs. thickness of liquid xenon.

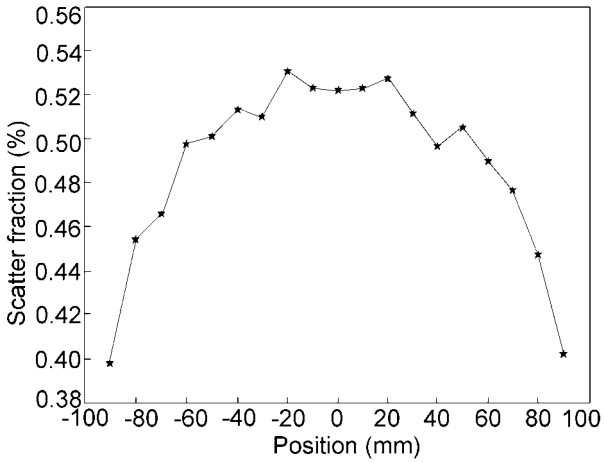

Fig. 3. Scatter fraction vs. axial position of line source.

In the next set of numerical experiments the axial position of the line source is varied to study the sensitivity and scatter fraction of the scanner. The line source is placed at the center of the scanner, parallel to the axis and is moved along the axis.

The scatter fraction (SF) is a principal factor affecting image contrast and image quantification. This quantity can be calculated as given below [29]:

$$\text{SF} = S/(S + T), \tag{2}$$

where S and T are the scatter, and true coincidence count rates, respectively.

Figure 3 shows that the scatter fraction varies from 0.4 for a line source which is 90 mm off-center of the scanner to 0.52 mm for a line source at the central region. As it can be observed in Fig. 4 the sensitivity has almost exactly opposite trend to the scatter fraction, reaching a minimum of 1.1% at the center and a maximum of 2.1% at the edge.

In the last set of simulations, the effect of detector material is studied. The spherical geometry of the scanner is kept unchanged, while the detector material varies from LXe to BGO and LSO. The thickness of the detectors also varies. The physical properties and the thickness of these scintillators are listed in Table 3.

The signal-to-noise ratio (SNR) in the final reconstructed image from a PET system is proportional to

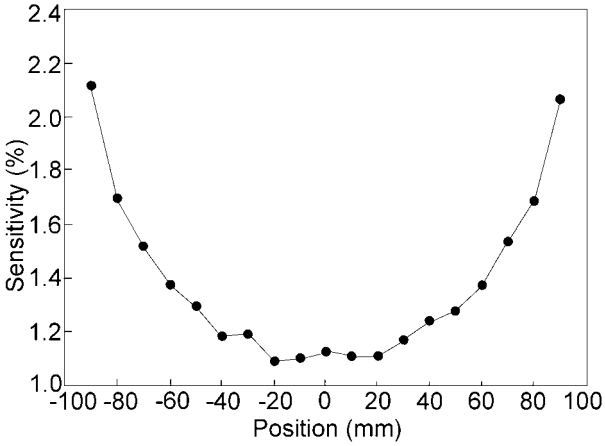

Fig. 4. Sensitivity vs. axial position of line source.

Table 3. Setting of digitizer BGO, LSO, LXe in SBPET

Material	BGO	LSO	LXe
Dead time (ns)	3600	500	25
Coincidence window (ns)	12	6	2.2
Energy resolution (%)	12	9.1	22
Thickness (mm)	30	20	100
Energy window (KeV)	350–650	350–650	400–600

noise equivalent count rate (NECR), this quantity is calculated from [29]:

$$\text{NECR} = T^2/\text{T} + S + 2kR, \tag{3}$$

where T, R and S are the true, random and scatter coincidence count rate, respectively, k is the fraction derived from the injected activity concentration. This value is obtained by using a 20 cm cylindrical phantom and uniform source activity placed at the center of the field of view, measuring prompt coincidence count. The true event (T) is determined by subtracting scatter (S) and random (R) event from prompt events. NECR serves as the relevant parameter to compare the performance of different PET systems.

In Fig. 5 NECR as a function of activity is presented for three different detector materials. It is shown that NECR for LXe in the highest activity is shown to be almost 2.8 and 3.6 times higher than NECR for LSO and BGO detectors, respectively. This means LXe detectors will provide highest imaging signal-to-noise ratio (SNR) amongst all of the scintillator materials. The relatively high NECR of LXe in low activity concentration is important for the visibility of small tumors in brain.

It should be noted that the energy resolution of LXe depends on the dimension of detector and photomultiplier. This value was measured and reported in previous experimental studies. The reported energy resolution is 13.8% in a WB-PET [8, 22], 15–35% in TOF-PET [11], 29.9% [27], and 13–17% in [7]. Although, in the present simulations the energy resolution is pessimistically estimated as 22% [5], LXe performs better compared to LSO and BGO.

In Fig. 6, the random, scattered, true, and total count rates are presented. Lower random count rates for

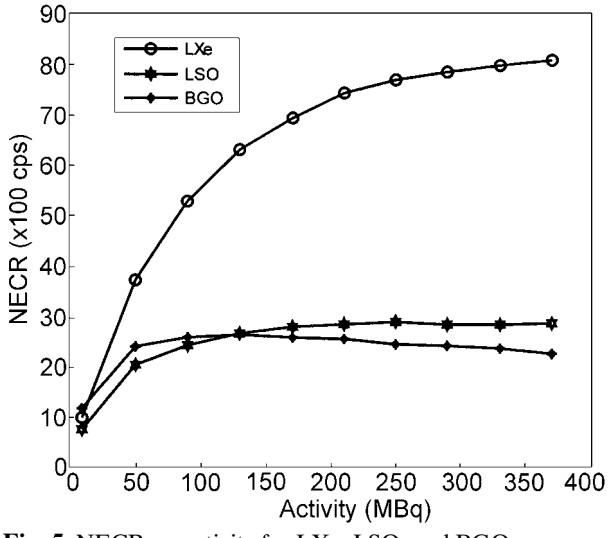

Fig. 5. NECR vs. activity for LXe, LSO, and BGO.

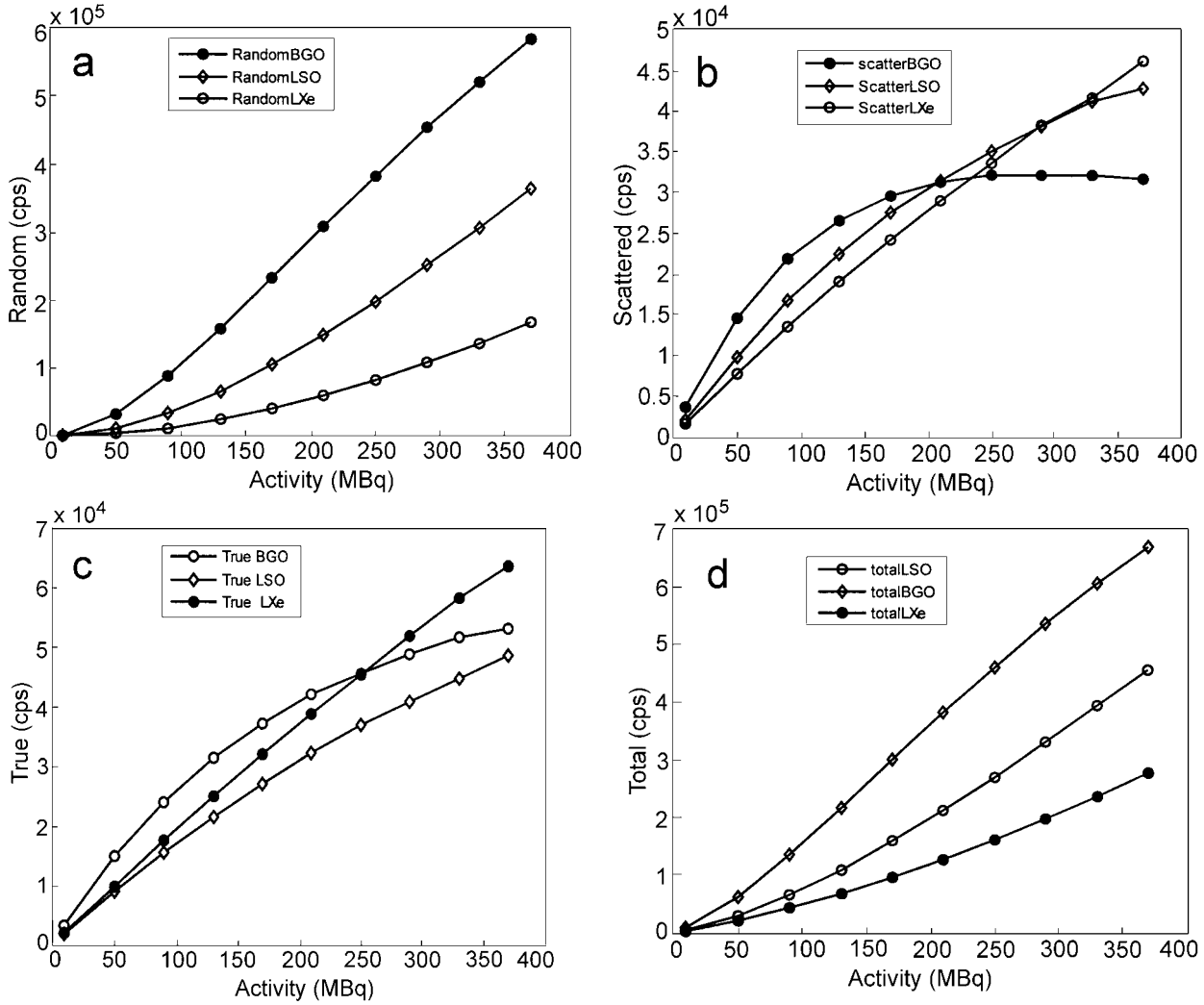

Fig. 6. Random (a), scattered (b), true (c) and total (d) count rates for BGO, LSO, and LXe.

LXe is shown in Fig. 6a which can explain the desirable signal-to-noise ratio of this material at high-count rates. Additionally, it can be observed that LXe has the highest scatter and true counts at high activity range.

To compare the performance of SBPET to an existing high-resolution scanner with comparable scanner size, ECAT HRRT is selected. The numerical results show SBPET has a higher sensitivity (1.14%) compared to that of ECAT HRRT (1.0%), while the spatial resolution of SBPET (~2.7 mm FWHM) is comparable to that of ECAT HRRT with ± 10% difference [2].

Conclusion

The idea of a PET system with spherical scanner design and LXe detectors (SBPET) is explored in the present work.

SBPET has a sensitivity of 1.14% and a spatial resolution of ~2.7 mm FWHM which is superior to ECAT HRRT. An increase, by a factor of about 5, in the counting rate of the present tomograph compared to WB-PET and the relatively high NECR in high count rate are other advantages of the new system, which would improve the image quality.

In the future we are planning to replace the NEMA phantom model by a more sophisticated Hoffman brain phantom and to make accurate measurements of spatial resolution of SBPET using the STIR tool.

Acknowledgment. The authors wish to thank Dr Thomas Ruth, Director of the UBC/TRIUMF PET programme at University of British Columbia, Vancouver, Canada for his continuous support. The authors are also gratefully indebted to the technical staff of UBC hospital for their contribution to this work.

References

1. Balldini C, Bemporad FC, Doke T (2004) Liquid Xe scintillation calorimetry and Xe optical properties. arXiv:physics/0401072
2. Bataille F, Comtat C, Jan S, Trebossen R (2004) Monte Carlo simulation for the ECAT HRRT using GATE. Nuclear Science Symp Conf Record IEEE 4:2570–2574
3. Buvate I, Castiglioni I (2002) Monte Carlo simulation in SPET and PET. J Nucl Med 46:48–61
4. Chepel V, Lopes MI, Kurchenkov A, Ferreira Marques R, Policarpo AJPL (1997) Performance study of liquid xenon detector for PET. Nucl Instrum Methods A 392:427–432
5. Chepel V, Lopes M, Solvov V, Ferreira Marques R, Policarpo AJPL (2001) Development of liquid xenon detector for medical imaging. World Sci (28-11-02) 11;58:1–13

6. Collot J, Jan S (2001) A liquid xenon PET camera for neuro-science. In: Proc of the 9th Int Conf Calorimetry in High Energy Physics. arXiv.org/pdf/physics/0211117
7. Cussonneau JP, Carlier T, Couturier O *et al*. (2005) Simulation and evaluation of a new PET system based on Liquid Xenon as detection medium. ICDL IEEE Int Conf, pp 357–360
8. DeGrado TR, Turkington TG, Williams JJ, Stearn CW, Hoffman JM, Coleman RE (1994) Performance characteristics of a whole-body PET scanner. J Nucl Med 35:1398–1406
9. Del Guerra A, Bisogni MG, Damiani C, Di Domenico G, Marchesini R, Zavattini G (2000) New developments in photo detection for medicine. Nucl Instrum Methods A 442:18–25
10. Derenzo SE, Weber MJ, Bourret-Courchesne E, Klintenberg MK (2003) The quest for the ideal inorganic scintillator. Nucl Instrum Methods A 505:111–117
11. Doke T, Kikuchi J, Nishikido F (2006) Time of flight positron emission tomograghy using liquid xenon scintillation. Nucl Instrum Methods A 569:863–871
12. Eijk CWE van (2002) Inorganic scintillators in medical imaging. Phys Med Biol 47:R85–R106
13. Gallin-Martel ML, Martin P, Mayet F *et al*. (2006) Experimental study of a liquid xenon PET prototype module. Nucl Instrum Methods A 563:225–228
14. Herzog H, Tellmann L, Hocke C *et al*. (2004) NEMA NU2-2001 guided performance evaluation of four Siemens ECAT PET scanners. IEEE Trans Nucl Sci 51;5:2662–2669
15. Hoffman EJ, Phelps ME, Huang SC (1983) Performance evaluation of a positron tomograph designed for brain imaging. J Nucl Med 24:245–257
16. http://www.oken.co.jp/web_oken/Mgf2_jp.htm
17. Humm JL, Rosenfeld A, Del Guerra A (2003) From PET detector to PET scanners. Eur J Nucl Med Mol Imag 30:11:1574–1597
18. Jan S, Collet J, Tournefier E (2000) A liquid xenon PET camera – simulation and position sensitive PMT test. Nuclear Science Symp Conf Record IEEE, pp 23–26
19. Jan S, Santin G, Strul D *et al*. (2004) Gate: a simulation toolkit for PET and SPECT. arXiv:physics/0408109
20. Karimian A, Thompson CJ, Sarkar S *et al*. (2004) A dedicated PET system for breast imaging (CYBPET). Nuclear Science and Medical Imaging Symp Conf Record IEEE 4:2339–2341
21. Karimian A, Thompson S, Sarkar S, Raisali G, Pani R (2005) CYBPET: A cylindrical PET system for breast imaging. Nucl Instrum Methods Phys Res A 545:427–435
22. Lartizien C, Comtat C, Kinahan PE, Ferreira N, Bendriem B, Trebossen R (2002) Optimization of injected dose based on noise equivalent count rates for 2- and 3-dimensional whole-body PET. J Nucl Med 43:1268–1278
23. Mortazavi N, Karimian A, Mostajaboddavati M (2006) Design of new dedicated brain PET system by Monte Carlo method. World J Nucl Med 5:S215, 3653
24. Mortazavi Moghaddam N (2007) Design of a new dedicated brain PET system by GATE, EANM 2007, Kopinhag, Denmark: S-158, 179
25. Moses WW, Virador PRG, Derenzo SE, Huesman RH, Budinger TF (1997) Design of a high resolution, high-sensitivity PET camera for human brains and small animals. IEEE Trans Nucl Sci 44:1487–1491
26. NEMA (2000) Standards Publication NU 2-2000. National Electrical Manufactures Association, Washington, DC
27. Nishikido F, Doke T, Kikuchi J, Mori T (2004) Performance of a prototype of liquid xenon scintillation detector system for positron emission tomography. Japanese J Appl Phys 43;2:779–784
28. Nutt R (2002) The history of positron emission tomography. Mol Imag Biol 4;1:11–26
29. Saha GB (2004) Basics of PET imaging. Springer, New York
30. Santin G, Strul DE, Lazaro D, Simon L, Morel C (2002) Gate: A Geant4 – based simulation platform for PET and SPECT integrating movement and time management. Nuclear Science Symp Conf Record IEEE 2:1325–1329
31. Schmidtlein CR, Kirov AS, Nehmeh SA, Erdi YE (2006) Validation of gate Monte Carlo simulations of the GE advance/discovery LS PET scanner. Med Phys 33;1:198–208
32. Seguinot J, Braem A, Chesi E *et al*. (2005) Novel geometrical concept of high performance brain PET scanner: principle, design and performance estimates. Pre-print CERN PH EP/2004 050
33. Sossi V (2003) Positron emission tomography (PET) advances in neurological applications. Nucl Instrum Methods A 510:107–115
34. Thers D (2005) PET, imaging technologies and electronics. In: XeSAT Proceedings, Waseda University, Tokyo, Japan, pp 84–89
35. Thompson CJ, Yamamoto YL, Meyer E (1979) Positome II: A high efficiency positron imaging device for dynamic brain studies. IEEE Trans Nucl Sci 26;1:583–589
36. Townsend DW, Defrise M (1993) Image reconstruction methods in positron tomography. Academic Training Program of CERN, Report No 93-02, CERN, Division de Medicine Nuclear, Hospital Cantonal Universities de Geneve, Geneva, Switzerland
37. Wienhard K, Schmand M, Casey ME *et al*. (2003) The ECAT HRRT: performance and first clinical application of the new high resolution research tomograph. IEEE Trans Nucl Sci 49:104–110
38. Zaidi H, Montandon M (2005) Atlas guided non-uniform attenuation in cerebral 3D PET imaging. Neuro Image 25:278–286
39. Zaidi H, Montandon ML (2006) The new challenges of brain technology. Curr Med Imag Rev 2;15:3–13